

Doppler optical cardiogram gated 2D color flow imaging at 1000 fps and 4D *in vivo* visualization of embryonic heart at 45 fps on a swept source OCT system

Adrian Mariampillai¹, Beau A. Standish¹, Nigel R. Munce¹, Cristina Randall³, George Liu³, James Y. Jiang⁴, Alex E. Cable⁴, I. Alex Vitkin^{1,2,3}, Victor X.D. Yang^{3,5,6}

Depts. of ¹Medical Biophysics and ²Radiation Oncology, University of Toronto, Toronto, ON, M5G 2M9, Canada

³Ontario Cancer Institute/University Health Network, Toronto, ON, M5G 2M9, Canada

⁴Thorlabs, Inc. 435 Route 206 North, Newton, NJ 07860

⁵Dept. of Physics, Ryerson University, Toronto, ON, M5B 2K3, Canada

⁶Imaging Research, Sunnybrook Health Science Centre, Toronto, ON, M4N 3M5, Canada

victor.yang@utoronto.ca

Abstract: We report a Doppler optical cardiogram gating technique for increasing the effective frame rate of Doppler optical coherence tomography (DOCT) when imaging periodic motion as found in the cardiovascular system of embryos. This was accomplished with a Thorlabs swept-source DOCT system that simultaneously acquired and displayed structural and Doppler images at 12 frames per second (fps). The gating technique allowed for ultra-high speed visualization of the blood flow pattern in the developing hearts of African clawed frog embryos (*Xenopus laevis*) at up to 1000 fps. In addition, four-dimensional (three spatial dimensions + temporal) Doppler imaging at 45 fps was demonstrated using this gating technique, producing detailed visualization of the complex cardiac motion and hemodynamics in a beating heart.

© 2007 Optical Society of America

OCIS codes: (170.4500) Optical coherence tomography; (170.3880) Medical and biological imaging; (100.68900) Three-dimensional image processing; (110.4500) Optical coherence tomography; (170.3340) Laser Doppler velocimetry.

References and links

1. M. A. Choma, S. D. Izatt, R. J. Wessells, R. Bodmer, and J. A. Izatt, "Images in cardiovascular medicine: in vivo imaging of the adult *Drosophila melanogaster* heart with real-time optical coherence tomography," *Circulation*, **114**, e35-e36 (2006).
2. S. A. Boppart, G. J. Tearney, B. E. Bouma, J. F. Southern, M. E. Brenzinski, and J. G. Fujimoto, "Noninvasive assessment of the developing *Xenopus* cardiovascular system using optical coherence tomography," *Proc. Natl. Acad. Sci.* **94**, 4256-4261 (1997).
3. S. Yazdanfar, M. Kulkarni, and J. Izatt, "High resolution imaging of in vivo cardiac dynamics using color Doppler optical coherence tomography," *Opt. Express* **1**, 424-431 (1997).
4. V. X.D. Yang, M. Gordon, E. Seng-Yue, S. Lo, B. Qi, J. Pekar, A. Mok, B. Wilson, and I. Vitkin, "High speed, wide velocity dynamic range Doppler optical coherence tomography (Part II): Imaging in vivo cardiac dynamics of *Xenopus laevis*," *Opt. Express* **11**, 1650-1658 (2003).
5. S. A. Boppart, G. J. Tearney, B. E. Bouma, J. F. Southern, M. E. Berzinski and J. G. Fujimoto, "Noninvasive assessment of the developing *Xenopus* cardiovascular system using optical coherence tomography," *Proc. Natl. Acad. Sci. USA*, **94**, 4256-4261 (1997).
6. T. Mesud Yelbuz, M. A. Choma, L. Thrane, M. L. Kirby and J. A. Izatt, "A new high-resolution imaging technology to study cardiac development in chick embryos," *Circulation*, **106**, 2771 (2002).
7. M. W. Jenkins, F. Rothenberg, D. Roy, V. P. Nikolski, Z. Hu, M. Watanabe, D. L. Wilson, I. R. Efimov, and A. M. Rollins, "4D embryonic cardiography using gated optical coherence tomography," *Opt. Express* **14**, 736-748 (2006).

8. D. L. Marks, T. S. Ralston, and S. A. Boppart, "Three-dimensional optical coherence tomography of the embryonic murine cardiovascular system," *J. Biomed. Opt. Special Issue on Cardiovascular Photonics*, **11**, 021014 (2006).
9. S. Yazdanfar, A. M. Rollins and J. A. Izatt, "Imaging and velocimetry of the human retinal circulation with color Doppler optical coherence tomography," *Opt. Lett.* **25** 1448-1450 (2000).
10. Z. P. Chen, T. E. Milner, D. Dave and J. S. Nelson, "Optical Doppler tomographic imaging of fluid flow velocity in highly scattering media," *Opt. Lett.* **22** 64-66 (1997).
11. A. W. Schaefer, J. J. Reynolds, D. L. Marks, and S. A. Boppart, "Real-time digital signal processing-based optical coherence tomography and Doppler optical coherence tomography," *IEEE Trans. Biomed. Eng.* **51** 186-190, (2004).
12. B. Vakoc, S. Yun, J. de Boer, G. Tearney, and B. Bouma, "Phase-resolved optical frequency domain imaging," *Opt. Express* **13**, 5483-5493 (2005).
13. R. Huber, D. C. Adler, and J. G. Fujimoto, "Buffered Fourier domain mode locking: unidirectional swept laser sources for optical coherence tomography imaging at 370,000 lines/s," *Opt. Lett.* **31**, 2975-2977 (2006).
14. V. XD. Yang, M. Gordon, B. Qi, J. Pekar, S. Lo, E. Seng-Yue, A. Mok, B. Wilson, and I. Vitkin, "High speed, wide velocity dynamic range Doppler optical coherence tomography (Part I): System design, signal processing, and performance," *Opt. Express* **11**, 794-809 (2003).
15. V. XD. Yang, N. Munce, J. Pekar, M. L. Gordon, S. Lo, N. E. Marcon, B. C. Wilson and I. A. Vitkin, "Micromachined array tip for multifocus fiber-based optical coherence tomography," *Opt. Lett.* **29**, 1754-1756 (2004).
16. E. Chérin, R. Williams, A. Needles, G. Liu, C. White, A. S. Brown, Y-Q. Zhou and F. S. Foster, "Ultrahigh frame rate retrospective ultrasound microimaging and blood flow visualization in mice in vivo," *Ultrasound Med Biol.* **32**, 683-691 (2006).
17. R. Huber, M. Wojtkowski, J. G. Fujimoto, J. Y. Jiang, and A. E. Cable, "Three-dimensional and C-mode OCT imaging with a compact, frequency swept laser source at 1300 nm," *Opt. Express* **13**, 10523-10538 (2005).
18. W. A. Reed, M. F. Yan, and M. J. Schnitzer, "Gradient-index fiber-optic microprobes for minimally invasive in vivo low-coherence interferometry," *Opt. Lett.* **27**, 1794-1796 (2002).
19. H. Li, B. A. Standish, A. Mariampillai, N. R. Munce, Y. Mao, S. Chiu, N. E. Marcon, B. C. Wilson, I. A. Vitkin, and V. XD. Yang, "Feasibility of Interstitial Doppler Optical Coherence Tomography for in vivo detection of microvascular changes during photodynamic therapy," *Lasers Surg. Med.* **38**, 754-761 (2006).
20. C. Kasai, K. Namekawa, A. Koyano, and R. Omoto, "Real-time two-dimensional blood flow imaging using an autocorrelation technique," *IEEE Trans. Sonics. Ultrason.* **32** 458-464 (1985).
21. M. Choma, M. Sarunic, C. Yang, and J. Izatt, "Sensitivity advantage of swept source and Fourier domain optical coherence tomography," *Opt. Express* **11**, 2183-2189 (2003).
22. J. F. de Boer, B. Cense, B. H. Park, M. C. Pierce, G. J. Tearney and B. E. Bouma, "Improved signal-to-noise ratio in spectral-domain compared with time-domain optical coherence tomography," *Opt. Lett.* **28** 2067-2069 (2003).

1. Introduction

Optical coherence tomography (OCT) is a high resolution (1 – 10 μm) imaging technique capable of visualizing structures to a depth of 2-3mm in soft tissues. The high spatial resolution provided by OCT has been used to study the developing cardiovascular system of various models in developmental biology including *Drosophila* (fruit fly) [1], *Xenopus laevis* (African clawed frog tadpole) [2-5], chick [6, 7] and mouse embryos [7, 8]. Doppler OCT (DOCT) is a functional extension of OCT, analogous to Doppler ultrasound, that can provide a flow sensitivity down to 10-100 $\mu\text{m/s}$ [9-12]. DOCT imaging of *Xenopus* embryos has been demonstrated at up to 16 frames per second (fps) [4]. In rodent models the heart rate can range from 200 to 500 beats per minute, which makes high temporal resolution a necessity for accurate characterization of cardiovascular function and development. To date, the highest in vivo structural OCT frame rate has been 360 fps [13]. High frame rate color Doppler flow imaging in OCT is very challenging due to the increased Doppler noise floor that accompanies the higher scanning optics velocities [14]. In Doppler ultrasound, this effect is negated through the use of arrayed transducers and electronic scanning such that no physical scanning motion is required. The concept of fiber array OCT systems has previously been described [15], but its use in DOCT has yet to be demonstrated.

The first demonstration of artificially increasing the imaging frame rate for OCT was by Yazdanfar *et al.*, who used a retrospective gating technique on the structural signal [3] to generate two-dimensional structural and color Doppler images from a time domain OCT system with a slow delay line frequency of 8 Hz. Jenkins *et al.* have used a prospective gating technique based on electrical pacing of excised hearts of chick and mouse embryo models to allow *ex vivo* 4D structural imaging at 16 fps [7]. Most recently, in the related field of high

frequency ultrasound (~50 μm resolution), Cherin *et al.* have performed *in vivo* structural and colour Doppler flow imaging of the mouse heart at 1000 fps using a retrospective gating technique based on a simultaneously acquired electrocardiogram (ECG) [16].

The retrospective gating techniques demonstrated by both Yandzafar and Cherin have the potential to increase the frame rate for color Doppler flow imaging while maintaining an acceptable noise floor. In this paper, we demonstrate a retrospective gating technique based on a Doppler optical cardiogram as it proved difficult to obtain an ECG signal from the *Xenopus*. In addition, for *in utero* mouse embryos, obtaining ECG signal would be problematic due to the difficulty in electrode placement and interference from the maternal heart or surrounding sibling's embryonic hearts. We demonstrate 1 kHz frame rates for both structural and Doppler images of the *Xenopus* cardiac dynamics as well as 4D (3D spatial + temporal) imaging at 45 fps. This was accomplished on a swept source (SS) OCT system, while using a separate Time Domain (TD) DOCT to provide the Doppler optical cardiogram.

2. Methods and materials

2.1 SS-DOCT system hardware

The Swept Source Doppler OCT (SS-DOCT) system is based on a commercially available frequency swept source (Thorlabs, SL1325-P16) that is centered at 1325 nm, with a FWHM of the optical spectrum of >100 nm, and an average output power of 12 mW. Further details about the swept source can be found in Ref. [17]. The OCT interferometer is based on a 90/10 Mach-Zehnder interferometer (MZI) where 90% of the power goes to the sample arm and 10% to the reference arm. The interference fringe signal is measured by a 15 MHz balanced photodetector (Thorlabs, PDB140C). Both the MZI clock signal and the interference fringe signal are digitized at 50 MS/s with 14-bit A/D resolution. The interference fringe data is recalibrated by using the MZI clock signal as described in Ref. [17] yielding ~1024 points per laser sweep. The SS-OCT system also outputs two waveforms, through a 16 bit digital to analog card (National Instruments, PCI-6731), to drive the XY galvanometer and scanning mirror assembly (Cambridge technology, 6210). The TD-OCT system is triggered by the start of the scanning driver waveform from the SS-DOCT system and streams the optical cardiogram data continuously to the hard drive. The SS-DOCT system acquires time-stamped B-mode structural images at 25 fps and streams the raw data to disk at the same time. Real time Doppler OCT imaging is performed at 12 fps using unidirectional wavelength sweeps from the laser. This imaging rate allowed for real-time feedback, which was required for tadpole positioning and visualization of breathing motion artifacts. Each B-mode image consisted of 512 A-scans per image. Prior to *in vivo* *Xenopus* cardiac imaging, the phase stability of the SS-OCT system was measured.

2.2 Doppler optical cardiogram hardware

A schematic of the imaging setup is shown in Fig. 1. The TD-OCT system has been previously described with a Michelson interferometer and a rapid scanning optical delay (RSOD) line at a 12.95 kHz resonant frequency [4]. The light source (Inphenix, IPSDM-1322) is centered at 1310 nm with ~55nm full width half maximum (FWHM) bandwidth and an output power of 22 mW. The interference signal was measured with a 10 MHz dual balanced photodetector (New Focus, 2117-FC). A 4.3 MHz electro-optic phase modulator is placed in the delay line providing stability for phase measurements while also providing the carrier frequency for in-phase (*I*) and quadrature (*Q*) demodulation. The *I* and *Q* signals were digitized with a 10 MHz data acquisition card (DAQ) (National Instruments, PCI-6115). The optical cardiogram was obtained via a previously described GRIN fiber imaging probe [18, 19].

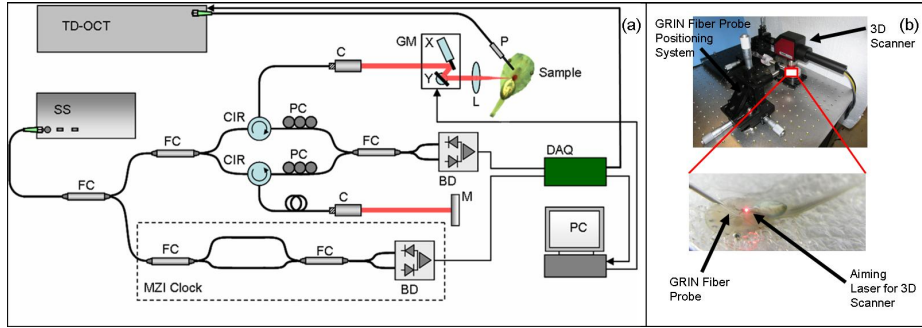


Fig. 1. Imaging setup. (a) SS: swept source, FC: fiber coupler, PC: polarization controller, CIR: circulator, C: collimator, M: mirror, BD: balanced detector, DAQ: data acquisition board, GM: galvo mirrors, L: lens, TD-OCT: time-domain OCT system, P:GRIN fiber probe.. (b) GRIN fiber probe positioned to image blood flow in one of the great vessels coming from the heart (tadpole in the ventral position). The TD-OCT system begins continuously acquiring data when it receives a trigger signal sent from the DAQ system of the SS-DOCT system.

2.3 Structural and Doppler signal processing

The results presented in this paper used only the forward wavelength (short to long) sweeps of the laser. Similar results can be produced from analyzing the backward wavelength sweeps of the laser. The recalibrated interference fringe pattern $F(k)$ can be processed to obtain both the structural and Doppler information encoded in the raw data. The Fourier transform of $F(k)$ gives the complex signal $I(y)+iQ(y)$. The structural image can be obtained by calculating the magnitude of the complex signal. A sliding window spatial averaging mask for the structural images defined in Eq. (1), is used to improve signal-to-noise (SNR) as has been described previously [4]. Briefly, M defines the size of the mask in the axial direction while N defines the size of the spatial averaging mask in the transverse direction. The B-mode structural images shown in this paper were generated using $N=4$ and $M=2$.

$$\langle S^2 \rangle = \frac{1}{MN} \sum_{m=1}^M \sum_{n=1}^N [I_{m,n}^2 + Q_{m,n}^2] \quad (1)$$

The frequency shift induced by moving scatterers in the direction of the incident laser beam can be estimated using the Kasai autocorrelation function [20]. The Kasai autocorrelation function measures phase shifts between two adjacent A-scans and is shown in Eq. (2).

$$\Delta\phi = \arctan \left\{ \frac{\frac{1}{M(N-1)} \sum_{m=1}^M \sum_{n=1}^{N-1} (I_{m,n+1}Q_{m,n} - Q_{m,n+1}I_{m,n})}{\frac{1}{M(N-1)} \sum_{m=1}^M \sum_{n=1}^{N-1} (Q_{m,n+1}Q_{m,n} + I_{m,n+1}I_{m,n})} \right\} \quad (2)$$

The spatial averaging mask values used for all B-mode Doppler images acquired by the SS-DOCT system were $N=8$ and $M=2$.

The phase shift induced by moving scatterers is displayed using a standard Doppler colormap with red and yellow indicating flow in the direction of the optical beam while blue and turquoise coloring indicate flow in the opposite direction in unaliased images. The maximum detectable phase shift without aliasing is $\pm\pi$, due to the complicated blood flow profiles and the presence of noise no attempt is made to phase unwrap images. Furthermore, due to the difficulty in determining the Doppler angle in the complicated structures of the heart we do not relate the phase shift to the velocity of moving scatterers.

2.4 Doppler optical cardiogram and retrospective gating

The RSOD frequency was measured at the beginning of each imaging session, allowing for accurate calculation of the elapsed time during data acquisition by counting the number of A-scans acquired. An example of the M-mode structural image through one of the two great vessels leaving the tadpole heart is shown in Fig. 2(a). The corresponding M-mode Doppler image is shown in Fig 2(b), the size of the averaging mask used to generate this image was $N=13$ and $M=1$. The pulsatile nature of the blood flow is clearly discernible in this image. Averaging the phase shift across the vessel shown in Fig 2(b) generates the cardiogram signal shown in Fig 2(c). A low pass finite impulse response filter was used to remove the high frequency noise with the result demonstrated in Fig. 2(d). One cardiac cycle was defined by the region between the vertical dotted lines. This allowed for the calculation of the duration in each cardiac cycle. The mean and standard deviation of the *Xenopus* cardiac cycle duration during the entire acquisition were calculated, and cardiac cycles with variations greater than 1.75 standard deviations were rejected.

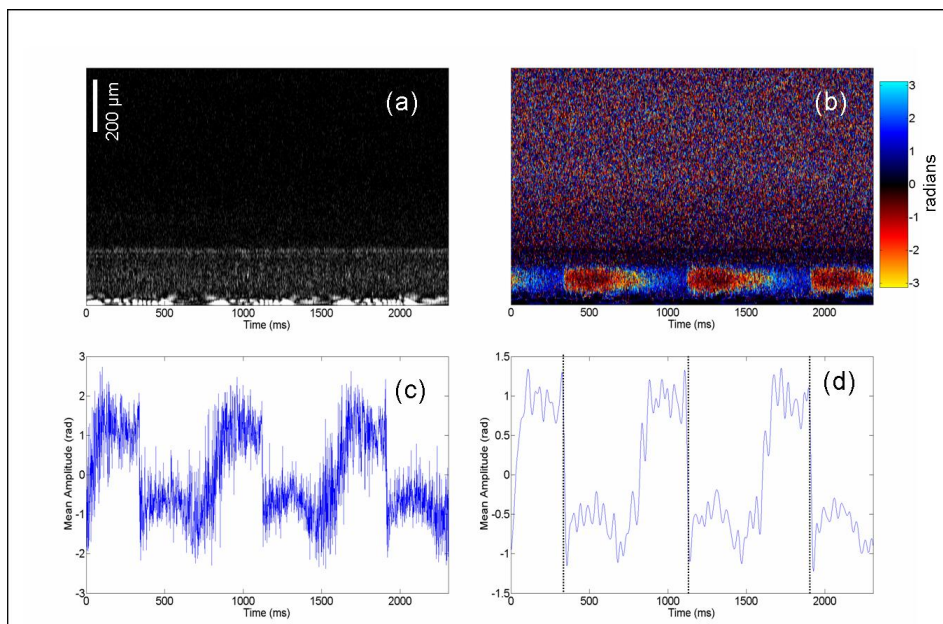


Fig. 2. Doppler optical cardiogram M-Mode data was collected from one of the two great vessels leaving the heart. Data was used to generate the optical cardiogram signal needed to retrospectively gate B-mode images. (a) Structural M-mode of great vessel. (b) Doppler M-mode of great vessel. (c) Raw optical cardiogram generated by averaging axially across the Doppler M-mode of the vessel. (d) Filtered cardiogram signal generated by filtering the raw signal with a 128th order finite impulse response low pass filter with 3dB cutoff at ~200 Hz and 80 dB stop band attenuation.

The overall system timing accuracy was 1 ms, and thus the highest frame rate achievable was 1000 fps for 2D movies. To achieve this maximum frame rate each cardiac cycle within the 1.75 standard deviation was divided into a number of equally spaced temporal bins determined by the mean cardiac cycle length over the image acquisition time of 2-3 minutes. For 1000 fps movies shown in section 3.2 the mean cardiac cycle length was approximately 800 ms and thus each cardiac cycle was divided into 800 temporal bins. B-Mode frames acquired by the SS-DOCT system were placed into the correct temporal bin using the time stamp attached to each frame. If multiple frames were found to originate from the same bin

only the first frame was kept. The frames were then re-ordered according to their temporal bin location to achieve the higher effective frame rate.

To reconstruct the 4D structural and Doppler models, the tadpole heart was imaged at approximately 150 different spatial locations. Each position was imaged for 15 seconds after which the 2D scanner stepped 10 μm and the process repeated. During each 15 second acquisition the cardiogram signal was also simultaneously collected with the TD-OCT system. An identical process to that described above was also followed for increasing the frame rate from 12 to 45 fps, using 36 temporal bins. The use of 36 temporal bin here was chosen as a trade off between good temporal resolution and performing manageable 4D reconstructions. The heart was then segmented in each of 36 different bins using the structural images. Masks were created to generate the surface reconstruction at each of the 36 bins as well as to segment the corresponding Doppler images.

2.5 Animal protocols

Xenopus laevis embryos were provided by Dr. Winklbauer in the Department of Zoology at the University of Toronto and were housed in standard conditions under an animal protocol approved by the institutional animal care committee at Princess Margaret Hospital, Toronto, Canada. Stage 51 tadpoles were anesthetized with 21°C (room temperature) Lidocaine solution diluted to 0.001% with tap water treated with Aqua Plus water conditioner. *Xenopus laevis* were allowed to sit in this solution for approximately 10 minutes before being placed in a shallow V-groove with a small amount of the solution. Images were then taken for approximately 1-2 hours and finally the animals were euthanized by anesthetic overdose.

In previous studies we have used 0.01% Tricaine as our anesthetic of choice. We chose Lidocaine in this study as a lower cost alternative. We compared its performance to Tricaine and found no significant degree of arrhythmia under our experimental conditions since over an imaging time of 180 secs, the cardiac cycle variation was only 2%. This may be attributed to the species difference between mammalian and amphibian cardiac systems.

The stage 51 *Xenopus* heart is a three-chambered heart consisting of two atria and one ventricle. Unlike the four-chambered mammalian heart the amphibian heart mixes oxygenated (left atrium) and deoxygenated (right atrium) blood inside the single ventricle. This mixture is pumped out of the ventricle to the systemic capillaries and the lungs through the common outflow tract known as the truncus arteriosus. The oxygenated blood from the lungs then returns to the left atrium while the deoxygenated blood from the systemic capillaries returns to the right atrium.

3. Results

3.1 Phase stability results

Prior to *Xenopus* imaging it was necessary to characterize the phase noise properties of the SS-DOCT system. The results are summarized in Fig. 3 and indicate a factor of five improvement (for $N=2$) in the intrinsic phase noise as compared to our TD-OCT system [14], as shown in Fig. 3(a). However, the overall Doppler noise in the system was still dominated by speckle modulation and sample arm scanning noise, which increased as a function of frame rate as shown in Figs. 3(b) and 3(c). The TD-OCT system used in this study, exhibits phase stabilities as a function of frame rate, that are similar to those found in Ref. [14].

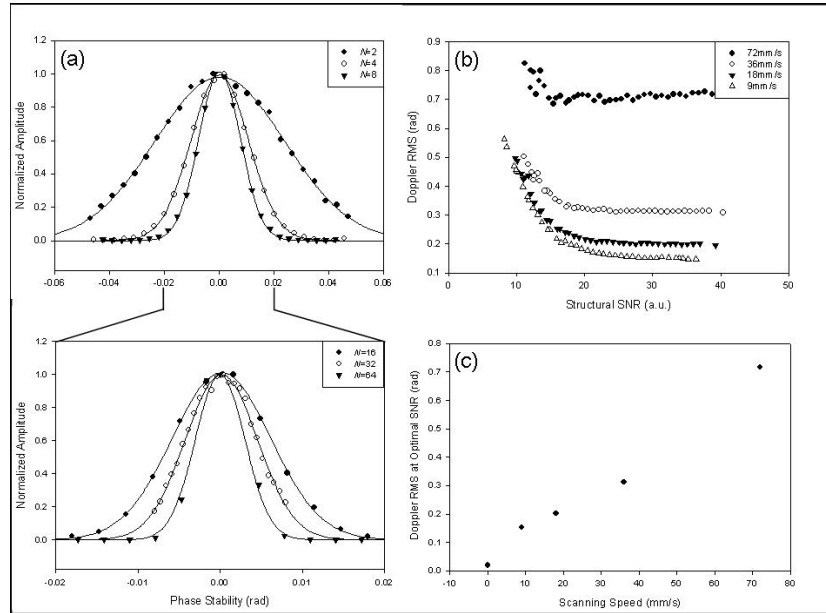


Fig. 3. (a). Normalized phase noise measured from a diffuse stationary reflector for various spatial averaging masks ($M=1, N=2, 4, 8, 16, 32, 64$). Each data set consists of measurements from 100,000 pixels and was fit with a Gaussian distribution. (b). Doppler noise floor measured in RMS when imaging stationary 0.5% Intralipid solution at 3, 6, 12, and 24 fps, or equivalently at 9, 18, 36, and 72 mm/s lateral scanning speed. The resultant images were split into 20 regions, each with different SNR for the structural OCT signal. The Doppler noise was measured in each region and plotted against the SNR. Spatial averaging mask values were $\{M=1, N=16\}$ for the 3 and 6 fps images and $\{M=1, N=8\}$ for the 12 and 24 fps images. (c). At optimal SNR, the minimum Doppler noise floor plotted against lateral scanning speed. For the remainder of the paper, the imaging was performed at 12 fps or 36 mm/s scanning speed.

3.2 Color doppler visualization at 1000 fps

An example of the original real-time 12 fps movie acquired by the SS-DOCT system is shown in Fig. 4. Structural intensity based thresholding of the Doppler images were performed in real-time to minimize Doppler noise, resulting in the movie in Fig. 4(b). This provided necessary feed back for proper positioning of the sample, identification of blood flow, and monitoring the tadpole for breathing motion during data acquisition to generate higher effective frame rate as described in Section 2.2.

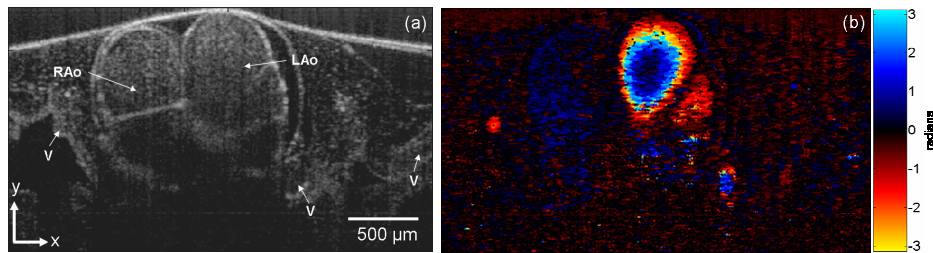


Fig. 4. SS-DOCT imaging of *Xenopus laevis* heart with real-time acquisition and display at 12 fps. (a) Cross-sectional structural movie at the level of the aortic arches (Movie figure_4a.mov, 220 kB). Vessel walls and blood pumped through the vessels are clearly seen. (b) Doppler movie at the same position, demonstrating flow through the vessels and the wall motion (Movie figure_4b.mov, 448 kB). RAo: right aortic arch, LAo: left aortic arch and V: pulmonary/gill vessels.

The resulting 1000 fps movies are shown in Fig. 5. Gated imaging at effectively 1000 fps gave us the option to implement a sliding window temporal averaging scheme over several

frames to improve the SNR in both the structural and Doppler images. Such a high effective frame rate allowed detailed capture of the complex cardiac motion and hemodynamics during the heart cycle. Even more importantly, this technique will allow for proper imaging of the mouse cardiovascular system, where heartbeat can exceed 6 beats per second.

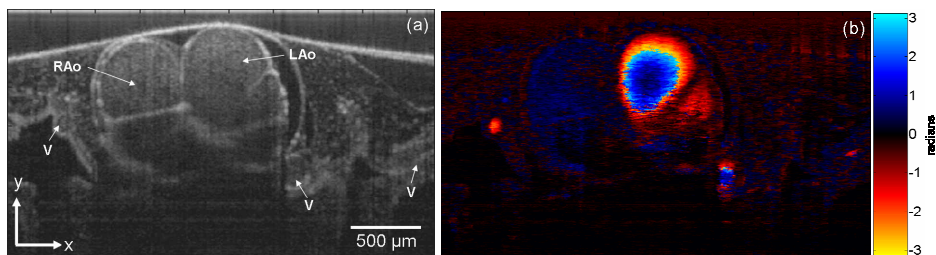


Fig. 5. Optical cardiogram gated movies at the same position as shown in Fig. 4 with an effective frame rate of 1000 fps, but played back at 30 fps. Sliding window temporal averaging was used to improve SNR. (a) Structural movie with a sliding window over 3 frames (Movie figure_5a.mov, 1793 kB). (b) Doppler movie with a sliding window over 5 frames (Movie figure_5b.mov, 1892 kB). Small artefacts (see discussion) contribute to the jittering motion, more prominently seen in the structural movie. Note the improved Doppler movie with a decreased noise level and more defined aliasing rings through the RAo and LAo. Notice the difference in Doppler shift between the blood flow and the vessel wall motion, both of which are present through out the cardiac cycle and visualized with high temporal resolution. Since the frame acquisition time is 83 ms, and the effective frame rate is 1000 fps, spatial-temporal artefacts are also present. These are demonstrated in (b), such as the right to left “flash” of red shifted Doppler frequencies in the vessel wall during the transition from late diastole to early systole, when the aortic arches move rapidly in the dorsal (downward) direction. The spatial-temporal effects are also depicted in Fig. 6, with data reconstruction in the x-t plane.

Furthermore, the left and right arches traverse through different angles (which changes during the cardiac cycle); these angles represent different incident Doppler angles to the optical axis. In addition, since the branching point moves into and out of the 2D imaging plane, with the downstream branches (especially of the right aortic arch) pointing in different directions, positive and negative Doppler frequencies are observed due to this diverging flow.

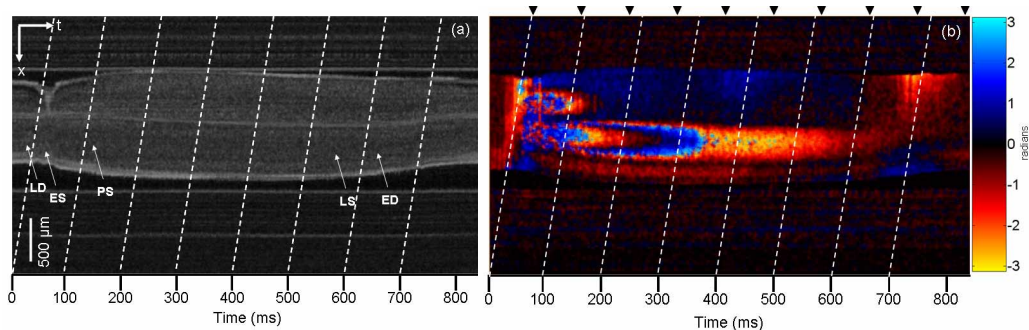


Fig. 6. Reconstructed 1000 fps data in the x-t plane, played back as movies through the y axis. (a) Structure movie (Movie figure_6a.mov, 4079 kB). (b) Doppler movie (Movie figure_6b.mov, 5309 kB). LD: late diastole, ES: early systole, PS: peak systole, LS: late systole, ED: early diastole. Equal-temporal lines (dash) every 100 ms are drawn. Note the spatial-temporal effects occur in the orientation parallel to the equal-temporal lines, as expected. Black arrow heads indicate the original 12 fps data acquisition time points, which are much more sparse when compared to the gated data. The fast hemodynamic changes during the cardiac cycle, especially during ES and PS phases, are better visualized with the gated data, demonstrating the rapid acceleration of flow from approximately 0 to 22 kHz (0 to 17.3 radians) Doppler shift within 60 ms.

The difference in flow pattern between the right and left aortic arches further exemplifies the need of 4D imaging to fully visualize and comprehend the complex nature of cardiac hemodynamics, even in a simple amphibian model.

The 1000 fps B-mode structural and Doppler images can be reconstructed to provide details in different planes. An example is shown in Fig. 6, where the data is presented in the x-t plane for better visualization of the temporal flow pattern, and appreciation of the different phases of the cardiac cycle.

3.3 Three dimensional + temporal (4D) imaging of the tadpole heart

Starting from the head end of the tadpole heart, we acquired SS-DOCT and Doppler optical cardiogram data as described in section 2.2 at different slice positions towards the tail. Three examples of the 45 fps structural and Doppler movies generated are shown in Figs. 7-9.

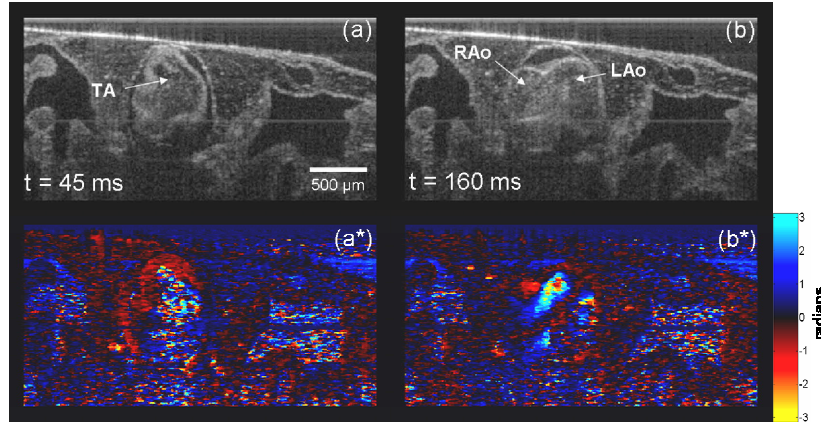


Fig. 7. Optical cardiogram gated structural movie (Movie figure_7a.mov, 1343 kB) at the level of truncus arteriosus (TA) branching into the left and right aortic arches (LAo, RAo) during early systolic (a) and peak systolic (b) phases of the cardiac cycle at 45 ms and 160 ms, respectively. The image acquisition is at 12 fps, the effective frame rate is 45 fps, and the movies are played back at 30 fps. The corresponding Doppler movies (Movie figure_7b.mov, 1780 kB) are shown in (a*) and (b*). These are shown without any threshold or spatial filtering to demonstrate the original system performance. Most of the noise in the Doppler background occurs at low structure intensity regions, which can be removed through simple thresholding performed in real-time.

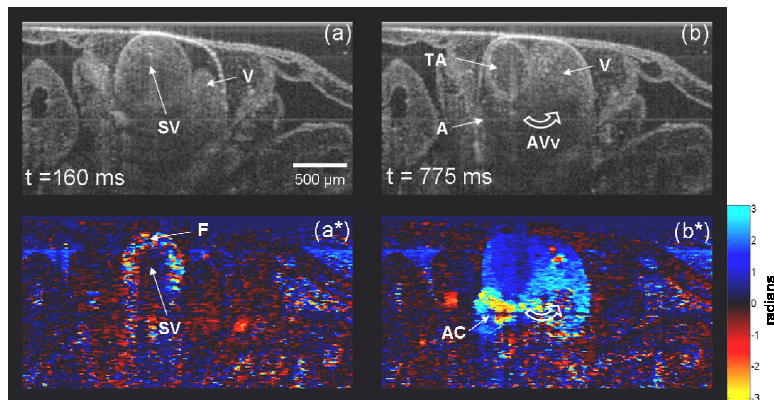


Fig. 8. Optical cardiogram gated structural movie (Movie figure_8a.mov, 1362 kb) at the level of spiral valve (SV) and atrio-ventricular valve (AVv) during peak systolic (a) and diastolic (b) phases of the cardiac cycle at 160 ms and 775 ms, respectively. Imaging conditions are identical to Fig. 7 and the corresponding Doppler movie (Movie figure_8b.mov, 1809 kB) is shown in (a*) and (b*). While the truncus arteriosus (TA) is within the imaging plane for the entire duration, the central ridge of the SV is only visible during the systolic phase due to the complex motion of the TA (as shown in Fig. 10). The blood flow (F) around the central ridge of SV is clearly visible during systole. In diastole, the atrium (A) provides blood flow (open arrow) to the ventricle (V) through the AVv, which is more prominent during atrial contraction (AC).

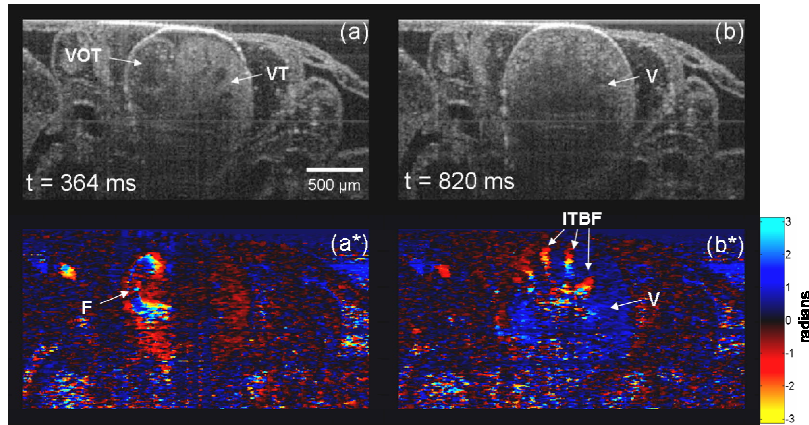


Fig. 9. Optical cardiogram gated structural movie (Movie figure_9a.mov, 1370 kB) at the level of ventricle (V) and ventricular outflow tract (VOT) during systolic (a) and diastolic (b) phases of the cardiac cycle at 364 ms and 820 ms, respectively. Imaging condition is identical to Fig. 7 and the corresponding Doppler movies (Movie figure_9b.mov, 1802 kB) are shown in (a*) and (b*). During systole, the blood flow in the VOT can be visualized, which is continuous with that in the TA. Ventricular trabeculae (VT) are also visible during systole. In diastole, blood flows into the ventricle and fills the space in between the trabeculae. This is demonstrated by the inter-trabecular blood flow (ITBF) in the Doppler image.

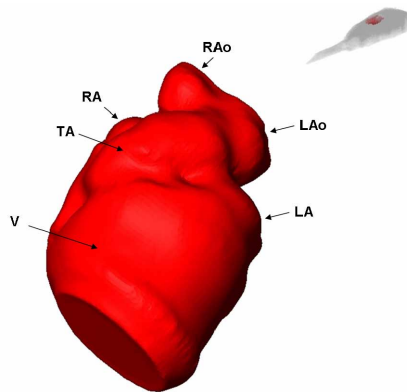


Fig. 10. 4D surface reconstruction (Movie figure_10.mov, 14908 kB) of the tadpole heart demonstrating the complex cardiac motion, and the relative position of the various components (V: ventricle, TA: truncus arteriosus, RA: right atrium, RAo: right aortic arch, LAo: left aortic arch, LA: left atrium) of the heart.

The entire 4D data set can then be used for other visualization reconstructions to better illustrate the complex cardiac motion during a heart beat cycle. Figure 10 shows a surface reconstruction of the tadpole heart, rotating while beating, to demonstrate the dynamic anatomical relationships. For example, the truncus arteriosus (TA) oscillates over a significant distance relative to the right and left atria (RA and LA), which are situated more posterior. During each cardiac cycle, the TA not only changes position, but its shape and diameter also vary periodically to accommodate the output blood flow from the ventricle (V).

Internal to the heart, the blood flow pattern and the heart wall motion velocity can also be visualized at different positions of the same cardiac phase (Fig. 11) or at the same position during different phases (Fig. 12).

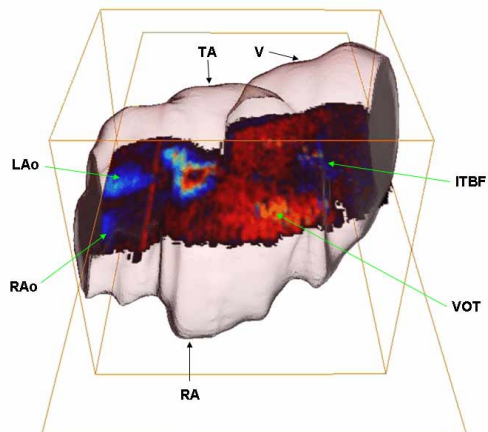


Fig. 11. Doppler shift within the tadpole heart during mid-systolic phase of the cardiac cycle, presented as a movie slice (Movie figure_11.mov, 12811 kB) moving through the heart in the ventral to dorsal direction. The surface of the heart is rendered semi-transparent to demonstrate the complex blood flow pattern in 3D.

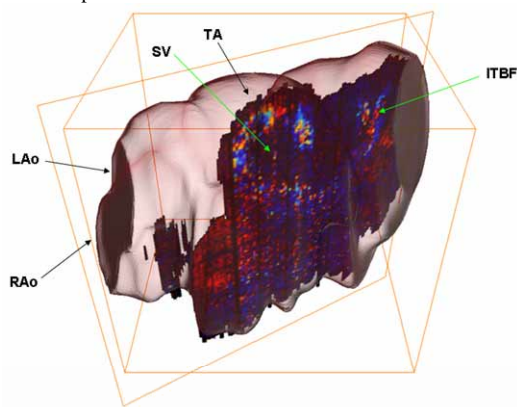


Fig. 12. Arbitrary oblique slice through the heart (Movie figure_12.mov, 3839 kB) to demonstrate the advantage of 4D Doppler imaging data set. Here the data visualization plane is chosen to be perpendicular to the TA for the majority of the cardiac cycle. Blood flow through the SV and ITBF in the ventricle are shown to illustrate the complex blood flow pattern.

4. Discussion

The demonstration above reports the highest effective frame rate in OCT and DOCT imaging of embryonic heart samples in which the motion is periodic over 2 to 3 minutes of time. It is also the first demonstration of combined 4D structural and blood flow OCT imaging, where the full complexity of the embryonic heart motion and blood flow can be visualized in detail. The Doppler optical cardiogram provides a novel method of tracking the highly periodic flow and motion in the cardiovascular system. In situations where conventional ECG signals are difficult to obtain, such as mouse embryos *in utero*, it provides a relatively easy way to accomplish gated 2D, 3D and 4D reconstructions. The techniques presented are suitable for *in utero* high speed 4D imaging and can be extended to visualize mouse embryo hearts at frame rates over 300 fps with low Doppler noise background.

Using a second OCT probe to provide the Doppler optical cardiogram also offers the possibility of imaging the peripheral vascular system, away from the heart where periodical structural motion may not be prominent. Hence, in organs such as the brain or kidney, single channel OCT with structural gating technique [3] will not be sufficient for 4D imaging. Acquisition of the gating signal on the same SS-DOCT system is an attractive option and thus we are currently in the process of modifying existing systems to perform this function. Since most commercially available DAQ cards have multiple analog input channels, systems can be modified to capture both the cardiogram and the B-mode images using a two-interferometer setup. The use of booster semi-conductor optical amplifiers may be necessary if the laser output power is not sufficient.

During data acquisition there are a number of effects that can lead to degradation in the temporal resolution of the reconstructions. This degradation effect, appears as “jittering”, tends to increase as the duration of data acquisition increases. We attribute this degradation to: (a) environmental effects such as evaporation of water in V-groove can cause a drift of the specimen; (b) small variations of heart beat period due to anesthetics; (c) breathing motion of the tadpole; and (d) de-correlation between the two DOCT systems. The de-correlation is limited by the accuracy of the two computer system clocks and fluctuations in the RSOD and SS sweeping frequencies. These effects limit the extent to which frame rates can be increased without introducing a significant amount of jitter. We found that the best compromise between jitter and high frame rates occurred at approximately 200-300 fps, corresponding to an acquisition time of approximately 20-30 seconds with the current setup. Using a two-channel setup, one could limit the de-correlation effect and allow higher effective frame rates in the future.

The Doppler noise floor in the 12 fps real-time acquisition and display mode of the SS-DOCT used in this study can be improved by using a swept wavelength source with higher sweeping frequency to increase the A-scan density (i.e., A-scans/mm) for a given frame rate. In addition, frequency domain mode locking [13] will also improve the phase stability and subsequently the accuracy of Doppler shift estimation.

The spatial-temporal artefacts observed in the high frame rate movies can be removed by re-sampling the data in the direction parallel to the equal-temporal lines. An alternate approach is to stop the lateral scanning and simply acquire M-mode data in a point-by-point fashion in the x-y plane. The advantage of such an approach is that the Doppler noise floor will be reduced to the intrinsic noise level of the SS-DOCT without contribution from the lateral scanning optics. The trade-off would be the loss of real-time monitoring capability of any breathing motion or other artefacts, and further post-processing detection of such effects would be required.

5. Conclusion

In conclusion, we have demonstrated a Doppler optical cardiogram gating technique to increase the effective frame rate for DOCT systems. This method allowed detailed Doppler imaging of the blood flow in the aortic arches of *Xenopus laevis* embryos at 1000 fps with 512 lines per frame on a SS-DOCT system. This image gating technique also yielded 4D imaging visualization of the complex 3D motion of the embryonic heart, and the hemodynamics therein, at 45 fps. These techniques may be used to image the cardiovascular system development in wild type and transgenic animal models, where phenotypic determination of cardiac morphology and function are important for studying the underlying genetics.

Acknowledgments

This work was supported by the Canadian Institutes of Health Research, Photonics Research Ontario, the Premier's Research Excellence Award, the Gordon Lang and the Samuel B. McLaughlin Foundations, and the Canadian Cancer Society through a grant from the National Cancer Institute of Canada. The authors acknowledge assistance from Dr. Rudolf Winklbaauer from the Department of Zoology, University of Toronto, ON, Canada, and Jurek Smolen and Xiao Jin from the Ontario Cancer Institute, Toronto, ON, Canada.